11

Isothermal and Non-isothermal Crystallization Kinetics of Poly(L-Lactide)/Carbonated Hydroxyapatite Nanocomposite Microspheres

Wen You Zhou[1], Bin Duan[2], Min Wang[2] and Wai Lam Cheung[2]
[1]*Discipline of Orthodontics, Faculty of Dentistry, The University of Hong Kong, 34 Hospital Road, Hong Kong,*
[2]*Department of Mechanical Engineering, The University of Hong Kong, Pokfulam Road, Hong Kong, China*

1. Introduction

Medical-profession-accepted and the US Food and Drug Administration (FDA)-approved biodegradable polymers have been used for tissue engineering applications over the last two decades due to their good biocompatibility and acceptable biodegradation properties. Poly(L-lactide) (PLLA) is a linear aliphatic biodegradable polymer and has been widely studied for use as a scaffolding material for human body tissue regeneration (Wei and Ma 2004; Chen, Mak et al. 2006; Wang 2006). The enzymatic and non-enzymatic hydrolysis rate of PLLA strongly depends on its chemical properties (such as molecular weight and weight distribution) and physical properties (such as crystallinity and morphology). Crystallinity plays an important role in the degradation behavior of biodegradable polymers. It is well known that the crystallinity and morphology of semicrystalline polymers such as PLLA are greatly influenced by their thermal history. Therefore, the crystallization kinetics of PLLA should be carefully studied and correlated to its processing method as it forms a basis for the interpretation of the scaffold properties. The isothermal bulk crystallization kinetics of PLLA has been studied by a number of research groups, covering a temperature range from 70 to 165 °C (Marega, Marigo et al. 1992; Iannace and Nicolais 1997; Miyata and Masuko 1998; Di Lorenzo 2005). But only a few studies were conducted on the non-isothermal crystallization kinetics of neat PLLA. Miyata and Masuko (1998) reported that PLLA could not crystallize and remained amorphous when the cooling rate was higher than 10 °C/min. The knowledge on non-isothermal crystallization kinetics is useful for modelling real industrial processes such as cast film extrusion, which generally takes place at a non-constant cooling rate (Piorkowska, Galeski et al. 2006).

Particulate bioceramic reinforced polymer composites can combine the strength and stiffness of bioactive inorganic fillers with the flexibility and toughness of biodegradable organic matrices. Carbonated hydroxyapatite (CHAp) is a desirable bioactive material for bone substitution as it is bioresorbable and also more bioactive in vivo than stoichiometric hydroxyapatite. PLLA/CHAp nanocomposite has been developed and used for constructing bone tissue engineering scaffolds through selective laser sintering (SLS) (Zhou, Lee et al. 2007; Zhou, Lee et al. 2008). In the SLS process, the laser beam selectively fuses

powdered material by scanning cross-sections generated from a 3D digital description of the part (e.g. from a CAD file or scan data) on the surface of a powder bed. After each cross-section is scanned, the powder bed is lowered by one layer thickness, a new layer of material is applied on top, and the process is repeated until the part is completed. Sintering is a thermal fusion process for bonding particles into solid structures (German 1996). The physical process of SLS may involve multiple cycles of melting (full or partial) and crystallization of polymer to produce solid parts. In SLS, individual microspheres are melted by laser beam to different degrees. Most microspheres comprise an un-melted core, surrounded by a melted and crystallized polymer that bonds with other microspheres. The mechanical properties of tissue engineering scaffolds are strongly related to the thermal properties of semi-crystalline biodegradable polymers. In a separate development, Ignjatovic et al. (2004) used hot pressing to produce PLLA/hydroxyapatite (HAp) biocomposite for medical applications. They found that the crystallinity of PLLA decreased after the process time of hot pressing was increased. However, the crystallization kinetics of PLLA/HAp composite was not fully evaluated. Currently, little is known about the effects of nano-sized HAp or CHAp on PLLA crystallization behavior under isothermal or non-isothermal conditions. In order to better understand the in vitro behavior of the PLLA/CHAp nanocomposite scaffolds produced by SLS, it is necessary to study the crystallization kinetics of the nanocomposite and the neat PLLA. In the current investigation, the overall crystallization kinetics and spherulitic morphologies of neat PLLA and PLLA/CHAp nanocomposite were studied by means of differential scanning calorimetry (DSC) and polarized optical microscopy (POM). In the isothermal crystallization study, the sample was rapidly cooled from the melt and allowed to crystallize at a pre-fixed temperature. In the non-isothermal crystallization study, the sample was allowed to crystallize upon cooling at various rates from the melt to room temperature.

2. Materials and methods

2.1 Materials

The PLLA used was Medisorb® 100L 1A (Lakeshore Biomaterials, AL, USA) with an inherent viscosity of 1.9 dL/g. It was supplied in the pellet form: 1 mm in diameter and 3 mm in length. The Mn and Mw of this polymer were determined to be 1.23×10^5 and 2.21×10^5, respectively, by gel permeation chromatography (GPC) using N-methyl pyrrolidone as the solvent. The CHAp nanospheres were synthesized in-house using a nanoemulsion method without surfactants (Zhou, Wang et al. 2008). The mean particle size of the resultant CHAp nanoparticles was about 20 nm. Poly(vinyl alcohol) (PVA, Sigma-Aldrich, cold water soluble) was used as the emulsifier and dichloromethane (DCM, A.R.) used as the organic solvent to dissolve PLLA for microsphere fabrication.

2.2 Fabrication of PLLA microspheres

PLLA microspheres were fabricated using a conventional oil-in-water (O/W) emulsion/solvent evaporation technique (Zhou, Wang et al. 2007). The resultant PLLA microspheres were washed and lyophilized to obtain dry powders.

2.3 Fabrication of PLLA/CHAp nanocomposite microspheres

PLLA/CHAp nanocomposite microspheres were produced using a solid-in-oil-in-water (S/O/W) emulsion/solvent evaporation method as reported previously (Zhou, Wang et al.

2007). Briefly, the CHAp nanoparticles were dispersed in the PLLA-dichloromethane solution by ultrasonification and homogenization to form an S/O nanosuspension. The nanosuspension was mixed with PVA solution to fabricate PLLA/CHAp nanocomposite microspheres. PLLA/CHAp microspheres containing 10 wt% of CHAp nanoparticles was used in this investigation.

2.4 Thermal property measurement and crystallization study

The thermal properties of PLLA and PLLA/CHAp nanocomposites and their crystallization behavior were studied using a Perkin Elmer Pyris 6 differential scanning calorimeter (DSC, MA, USA) and with the heating and cooling rates of 10 °C/min. The apparatus was calibrated with pure indium and zinc standards at various scanning rates. Dry nitrogen gas at a flow rate of 20 mL/min was used to purge through the DSC cell during all measurements. A new sample was used for each measurement in order to eliminate the effect of thermal degradation. Each test was repeated three times to ensure accuracy. The effect of previous heat treatments (thermal history) can significantly affect the shape of the DSC curve for semicrystalline polymers. In order to compare the thermal data of PLLA with values found in the literature, a standardized thermal history is desirable and can be achieved by a heat-cool-reheat DSC method (Lever 2007). In this method, the first heating process destroys any previous thermal history (assuming the maximum temperature is sufficient to remove any remaining nuclei without causing sample degradation), the cooling process imposes a known thermal history on the sample, and the second heating process allows the sample to be measured with a known thermal history. In this investigation, the samples were heated from room temperature to 200 °C with a heating rate of 10 °C/min (step 1) and held there for 5 min to eliminate the thermal history (step 2, annealing). Then samples were quenched to room temperature at cooling rate of 40 °C/min (step 3) and re-heated to 200 °C to probe the melting point (step 4). The glass transition temperature (T_g) was determined before annealing; while the cold crystallization and melting temperature (T_{cc} and T_m, respectively) and the enthalpy of cold crystallization and fusion (ΔH_{cc} and ΔH_m, respectively) were determined after annealing. The crystallinity (X_c) of the PLLA matrix was calculated from the reheating DSC data using the following equation (Sosnowski 2001; Arnoult, Dargent et al. 2007):

$$X_c(\%) = \frac{\Delta H_m - \Delta H_{cc}}{X_{PLLA}\Delta H_m^0} \times 100 \quad (1)$$

where ΔH_m is the measured enthalpy of fusion, ΔH_{cc} is the cold crystallization enthalpy of PLLA during the heating process, X_{PLLA} is the PLLA weight percentage in the composite. ΔH_m^0 is the enthalpy change of 100% crystalline PLLA, which is 135 J/g, as was estimated by Miyata and Masuko (1998) from the linear relationship between exothermic enthalpy change with density.

2.5 Isothermal crystallization

To investigate the overall kinetics of isothermal melt crystallization, PLLA samples (weighing between 10 to 15 mg) were heated in the DSC from 30 to 200 °C at a rate of 80 °C/min and held at 200 °C for 5 min to allow through melting. They were then cooled at 50 °C/min to the predetermined crystallization temperatures (T_c) and allowed to crystallize. The high cooling rate of 50 °C/min was used to minimize crystallization of PLLA during

cooling (Di Lorenzo 2005). The heat evolved during crystallization was recorded as a function of time.

2.6 Polarized optical microscopy

The spherulitic morphologies of neat PLLA and PLLA/CHAp nanocomposites were observed using a polarized optical microscope (POM, Metallux II, Leitz, Germany) equipped with a hot stage (Leitz 350, Germany) and a temperature controller (Partlow, MIC 8200, USA). Samples weighing about 5 mg were sandwiched between two microscope cover slides and melted at 200 °C to form thin films. The samples were held at the same temperature for 5 min to destroy any thermal history and then cooled to isothermal crystallization temperatures of 110, 120 and 130 °C. The temperature of the hot stage was kept constant within 0.1 °C and optical photographs were taken using a digital color camera (Samsung, SCC-101 BP, China).

2.7 Non-isothermal crystallization

For non-isothermal melt crystallization, the samples were quickly heated from 30 to 200 °C at a heating rate of 80 °C/min and maintained at 200 °C for 5 min in the DSC cell to destroy any nuclei that might act as seed crystals. The samples were then cooled to 30 °C at constant rates of 0.5, 1.0, 2.5, 5.0, 7.5 and 10 °C/min, respectively. The exothermic crystallization peaks were recorded as a function of temperature.

3. Results and discussion

3.1 Thermal properties

The thermal properties of neat PLLA and PLLA/CHAp were needed for the crystallization kinetics analysis and therefore determined through DSC. Typical DSC curves of neat PLLA and PLLA/CHAp nanocomposites were shown in Fig. 1 (a), (b) and thermal characteristics were listed in Table 1. It can be seen that the addition of CHAp nanoparticles decreased the glass transition temperature (T_g) and cold crystallization temperature (T_{cc}) of PLLA and slightly increased its melting temperature (T_m). These results suggest that the CHAp nanoparticles promoted initial glass transition and cold crystallization of the PLLA matrix, indicating an enhanced crystallization ability of PLLA in the presence of CHAp, which might behave as nucleating agents. Similar observations were made recently in the PLLA/nano-clay system (Wu, Wu et al. 2007) with a decrease of T_g value of 1-2 °C. The addition of 10 wt% CHAp nanospheres reduces the T_g of PLLA by about 2.89 °C. It has suggested that nanosheet particles are much favorable for the improvement of thermal stability compared to more isotropic geometry fillers, such as nanospheres (Murariu, Da Silva Ferreira et al. 2007). However, the detailed mechanisms for the decreased T_g value of PLLA after addition of CHAp are not clear. ΔH_{cc} and ΔH_m represent the cold crystallization enthalpy and enthalpy of fusion, respectively, from which the absolute degrees of crystallinity, X_c, of melt-quenched PLLA and PLLA/CHAp can be calculated using Equation (1). In theory, the lowest possible value for X_c is zero, which is for totally amorphous polymers. The negative value for the neat PLLA is most likely a result of the accuracy level of the DSC experiment. A more realistic interpretation is that $X_c \approx 0$, i.e. the melt quenched PLLA was more or less amorphous. In fact, our result has confirmed Miyata and Masuko's result (1998) that PLLA could not crystallize and remained amorphous when cooled at rates higher than 10 °C/min. In the current investigation, the samples were quenched at the rate of 50 °C/min. In comparison, the PLLA/CHAp nanocomposite gave a small but non-negligible X_c value of 4%. One possible explanation is

that the CHAp nanoparticles acted as a nucleating agent and promoted limited amount of crystallization even under such rapid cooling condition. During the DSC tests, cold crystallization occurred, giving rise to ΔH_{cc}. The value of ΔH_{cc} for PLLA/CHAp is slightly lower than that of the neat PLLA. This is probably because some crystallizable material had been consumed during the cooling process and the amount left for the cold crystallization process had dropped. Finally, the slightly higher ΔH_m value of the nanocomposite, compared to neat PLLA, indicates that the CHAp nanoparticles enhanced the overall crystallinity of the PLLA matrix.

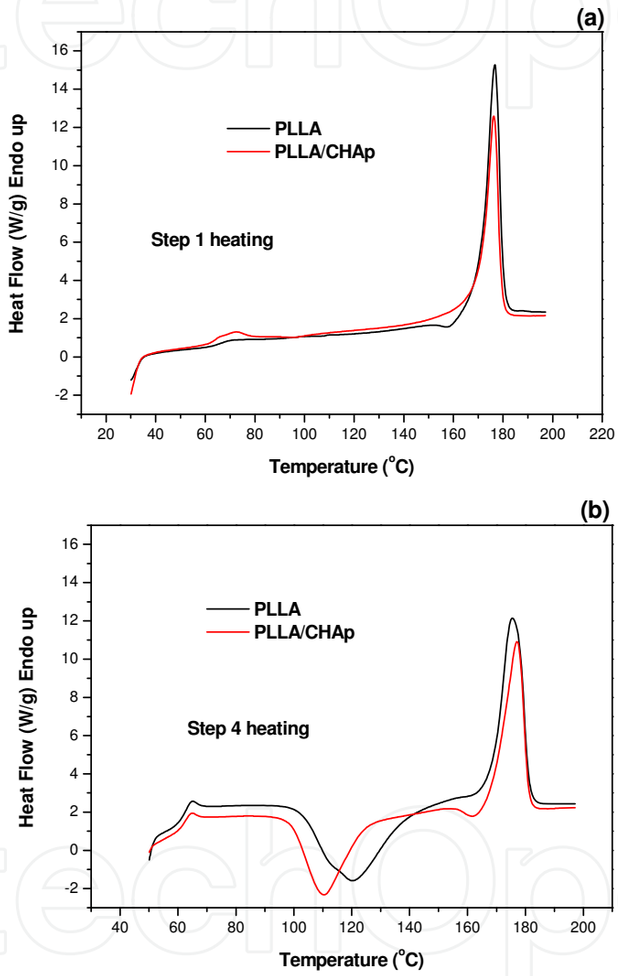

Fig. 1. DSC curves for the neat PLLA and PLLA/CHAp nanocomposites: (a) heating before annealing (step 1) and (b) heating after annealing (step 4).

Samples	T_g (°C)	T_{cc} (°C)	ΔHcc (J/g)	T_m (°C)	ΔHm (J/g)	X_c(%)
PLLA	66.74±0.15	120.13±0.11	37.98±2.75	175.22±0.24	36.79±0.43	-0.9
PLLA/CHAp	63.85±0.30	110.31±0.10	34.27[a]±2.91	177.1±0.33	39.59[a]±1.93	4.0

[a]Values of ΔH_{cc} and ΔH_m for PLLA/CHAp have been normalized to unit mass of PLLA.

Table 1. Thermal properties of melt-quenched neat PLLA and PLLA/CHAp nanocomposite.

3.2 Isothermal crystallization kinetics

The isothermal crystallization kinetics of neat PLLA and PLLA/CHAp nanocomposite was studied by cooling the melt rapidly (50 °C/min) to the crystallization temperature, ranging from 90 to 140 °C. The exothermal curves were then recorded as a function of crystallization time and the results are shown in Fig. 2. The values of crystallization enthalpy (ΔH_c) were obtained from the exothermal curves and are listed in Table 2. Clearly, ΔH_c increased with increasing crystallization temperature for both neat PLLA and PLLA/CHAp. At low isothermal crystallization temperatures, the addition of CHAp seemed to have little influence on the crystallization enthalpy of the PLLA matrix. At higher isothermal crystallization temperatures, however, it decreased the crystallization enthalpy significantly compared with that of neat PLLA. Such change may imply a drop in the amount of crystals formed or a lower degree of perfection of the crystals or both. The presence of a large amount of nano-sized CHAp particles (10 wt%) was likely to increase the melt viscosity, thus making it more difficult for the macromolecular chains to pack into perfect crystals.

Samples	T_c (°C)	ΔH_c (J/g)	ΔH_c^* (J/g)	n	k (min^{-n})	r^2	$t_{0.5}^*$ (min)	$t_{0.5}$ (min)
PLLA	90	22.31		2.60	1.66×10^{-3}	0.99998	10.23	10.18
	100	22.60		2.51	3.16×10^{-2}	0.99994	3.47	3.42
	110	32.95		2.67	2.51×10^{-2}	0.99988	3.51	3.46
	114	33.48		2.60	1.51×10^{-2}	1.00000	4.33	4.35
	116	36.97		2.59	1.26×10^{-2}	0.99998	4.63	4.70
	118	35.78		2.73	7.59×10^{-3}	1.00000	5.20	5.23
	120	42.28		2.80	5.25×10^{-3}	1.00000	5.65	5.72
	130	53.44		2.83	1.82×10^{-4}	0.99982	17.83	18.42
	140	51.34		2.91	7.94×10^{-6}	0.99994	48.67	49.87
PLLA/ CHAp	90	19.38	21.53	2.43	8.32×10^{-3}	0.99996	6.30	6.17
	100	22.27	24.74	2.47	1.15×10^{-1}	0.99998	2.10	2.07
	110	23.30	25.89	2.42	1.10×10^{-1}	0.99996	2.12	2.14
	114	27.88	30.98	2.52	4.90×10^{-2}	0.99996	2.83	2.86
	116	29.12	32.36	2.51	4.27×10^{-2}	0.99998	2.98	3.04
	118	30.94	34.38	2.57	3.10×10^{-2}	0.99994	3.30	3.35
	120	31.91	35.46	2.72	1.95×10^{-2}	1.00000	3.68	3.72
	130	37.23	41.37	2.83	2.29×10^{-3}	1.00000	7.55	7.53
	140	38.06	42.29	2.86	1.66×10^{-4}	0.99996	18.35	18.45

Notes: ΔHc^*: denotes the crystallization enthalpy normalized to unit mass of PLLA
r^2: denotes the coefficient of determination for the Avrami fit
$t_{0.5}^*$: denotes the half-life crystallization time obtained from the experiment (symbols in Fig. 4) $t_{0.5}$: denotes the half-life crystallization time calculated by Equation (7)

Table 2. Properties and parameters obtained from the isothermal crystallization of neat PLLA and PLLA/CHAp nanocomposite.

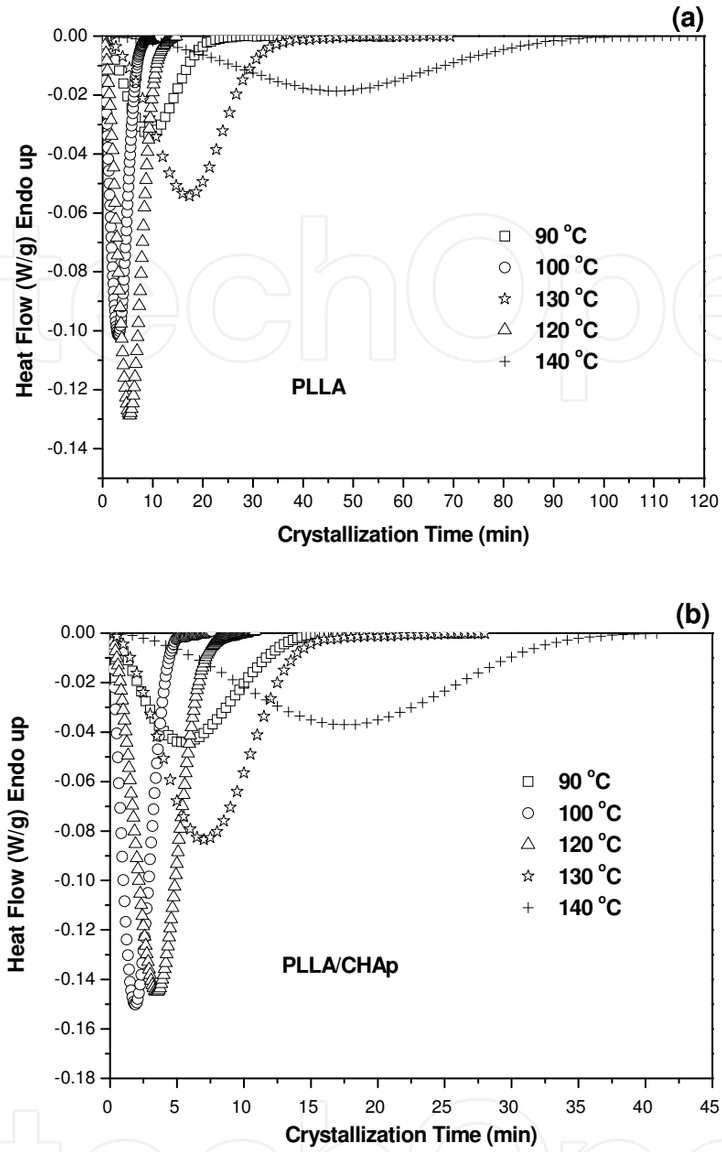

Fig. 2. DSC thermograms obtained from isothermal crystallization of (a) neat PLLA, and (b) PLLA/CHAp nanocomposite.

The kinetics of isothermal crystallization can be described by the well-known Avrami Equation (Piorkowska, Galeski et al. 2006). A time-dependent relative volumetric crystallinity X_t for an isothermal crystallization process can be expressed as:

$$X_t = 1 - \exp(-kt^n) \tag{2}$$

or

$$\log[-\ln(1 - X_t)] = \log k + n \log t \tag{3}$$

where t is the time, n is the Avrami exponent and k is the overall crystallization rate constant which contains contributions from both nucleation and growth. Parameters n and k can be obtained from the slope and intercept, respectively, of the Avrami plot of $\log[-\ln(1-X_t)]$ versus $\log t$. According to Lorenzo et al., (2007), the relative volumetric crystallinity (X_t) can be calculated as:

$$X_t = \frac{W_c}{W_c + (\rho_c/\rho_a)(1-W_c)} \tag{4}$$

where ρ_c and ρ_a are the fully crystalline and fully amorphous polymer densities, respectively. For commonly existed α form of PLLA, ρ_c = 1.283 g/cm^3 and ρ_a = 1.248 g/cm^3, (Oca and Ward 2007). The determination of the absolute crystallinity is not needed for the analysis of the crystallization kinetics, and the degree of relative mass crystallinity, W_c, can be calculated as:

$$W_c = \frac{\Delta H_t}{\Delta H_{total}} = \frac{\int_0^t (dH/dt)dt}{\int_0^\infty (dH/dt)dt} \tag{5}$$

taking ΔH_t as the enthalpy variation as function of the time spent at a given crystallization temperature, while ΔH_{total} is the maximum enthalpy value reached at the end of the isothermal crystallization process. Both quantities can be obtained from the isothermal curve by integration.

Fig. 3 displays the typical Avrami double-logarithmic plots for neat PLLA and PLLA/CHAp. The Avrami parameters n and k were obtained from the plots and are listed in Table 2. Fig. 4 shows the corresponding curves of relative degree of crystallinity with time (symbols) for neat PLLA and PLLA/CHAp obtained from the experimental crystallization isotherms as exhibited in Fig. 2. In a recent investigation (Lorenzo, Arnal et al. 2007), it was suggested that the choice of relative crystallinity range was very important for a good Avrami fit. The initial data points (X_t<3%) may not be accurate due to experimental errors during the primary crystallization stage and hence do not need to be under serious consideration. The secondary crystallization process produces nonlinearity in the Avrami plot so the relative crystallinity range should be chosen during the primary crystallization process. According to their study, a relative crystallinity range of 3 to 20% is sufficient for a good Avrami fit. In order to check the validity of the Avrami method for studying the isothermal crystallization kinetics of neat PLLA and PLLA/CHAp, the variations of the relative crystallinity (X_t) for the respective isothermal crystallization temperatures were calculated using the values of n and k listed in Table 2 and the results are shown as solid lines in Fig. 4. The calculated results fit very well with the experimental data, indicating that the Avrami method can be used to study the isothermal crystallization process in the current investigation in case some of the common problems were avoided (Lorenzo, Arnal et al. 2007). It can be seen from Table 2 that the coefficient of determination of the Avrami plot, r^2, is near unity, which also suggests a good fit between the theoretical and experimental results in the relative crystallinity range of 3 to 20% as recommended by Lorenzo et al. (2007). The valid values of n and k are essential to the Lauritzen-Hoffman analysis by using $t_{0.5}$ data.

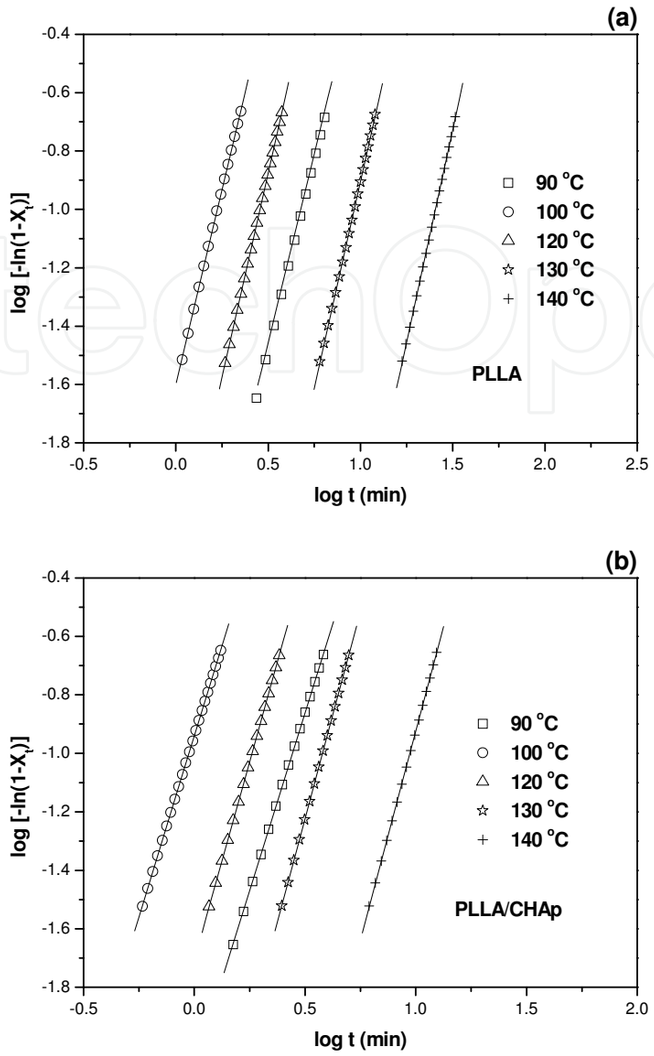

Fig. 3. Avrami plots for isothermal crystallization of (a) neat PLLA and (b) PLLA/CHAp nanocomposite (symbols: experimental data; solid lines: Avrami linear fit).

The Avrami exponent (n) is composed of two terms:

$$n = n_d + n_n \tag{6}$$

where n_d represents the dimensionality of the growing crystals and this quantity can only have, as values, the integer numbers 1, 2 or 3, corresponding to one-, two- or three-dimensional entities that are formed. In the case of polymers, only 2 and 3 are commonly obtained as they represent axialites (two dimensional lamellar aggregates) and spherulites (three dimensional aggregates of radial lamellae), respectively. The time dependence of the nucleation is represented by n_n. In principle, its value should be either 0 or 1, where 0 corresponds to instantaneous or heterogeneous nucleation and 1 to sporadic or homogenous nucleation. However, since in many cases the nucleation may be somewhere between completely instantaneous and completely sporadic nucleation, a noninteger Avrami exponent can be sometimes explained in this way (Lorenzo, Arnal et al. 2007). The Avrami n

for neat PLLA is from 2.6 to 2.9 in the isothermal temperature range of 90 to 140 °C; the Avrami n for PLLA/CHAp is from 2.4 to 2.9 in the same temperature range. The Avrami exponent close to 3 at high isothermal crystallization temperatures indicates a changing trend of PLLA crystal growth from two- to three-dimensional with instantaneous nucleation and athermal (Iannace and Nicolais 1997). The obtained n values were similar to those reported for neat PLLA (2.4-3.2 at T_c=90-125 °C by Tsuji et al. (2006), 2.8-3.2 at T_c=90-130 °C by Iannace and Nicolais (1997), 2.5-3.3 at T_c=90-130 °C by Kolstad (1996)). However, Miyata and Masuko (1998) reported an n value ca. 4 at T_c=110-132.5 °C. The differences can be attributed to the determination of the onset of crystallization or induction time, the establishment of the baseline and incomplete isothermal crystallization data, the effect of the cooling rate from the melt to the isothermal crystallization temperature and the relative degree of crystallinity range employed for the Avrami fitting (Lorenzo, Arnal et al. 2007).

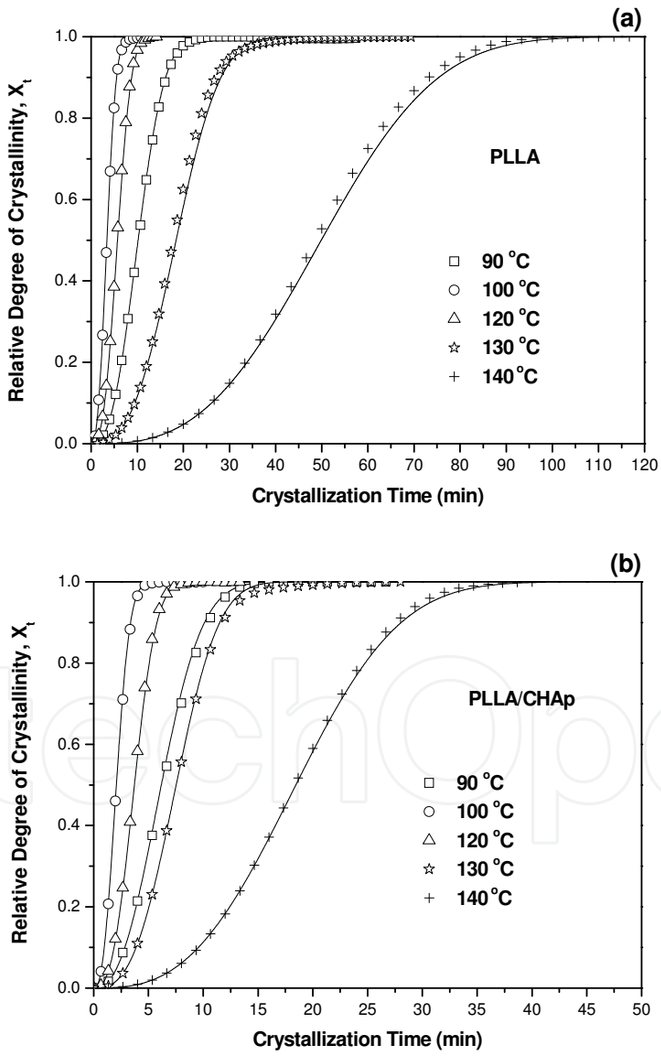

Fig. 4. Development of relative degree of crystallinity as a function of crystallization time for (a) PLLA, and (b) PLLA/CHAp nanocomposite. (Symbols: experimental data; solid lines: calculated crystallinity using Equation (2) and Avrami parameters n and k in Table 2.)

Also, the nucleation is seldom either athermal or simple thermal (Pethrick 2007). It can be seen from Table 2 that the values of Avrami exponent (n) of the PLLA/CHAp nanocomposite are lower than those of the neat PLLA for the same crystallization temperatures. One possible reason is that the large amount of CHAp nanoparticles might have affected the nucleation and growth mechanisms of the PLLA crystals. Better interpretation of the Avrami exponent requires more information about the specific nucleation and growth mechanisms of PLLA crystal, but at this stage we do not have such information.

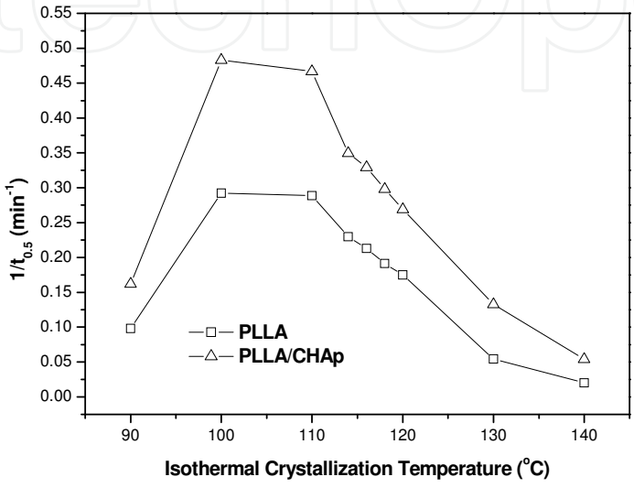

Fig. 5. Dependence of $1/t_{0.5}$ of PLLA and PLLA/CHAp nanocomposite on isothermal crystallization temperature.

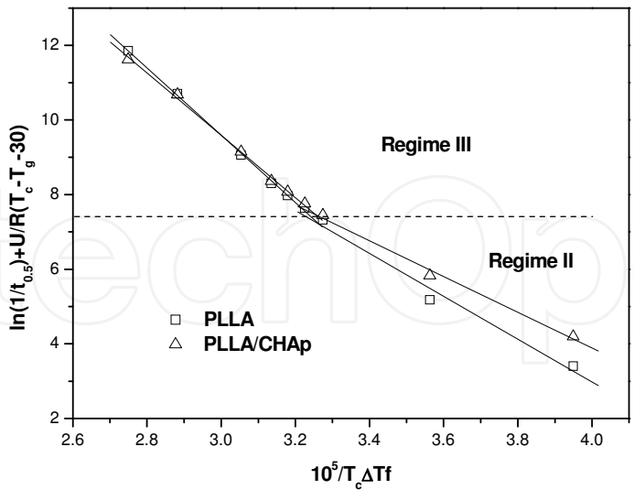

Fig. 6. Hoffman-Lauritzen plots for the estimation of nucleation parameters of neat PLLA and PLLA/CHAp nanocomposite (symbols: calculated data; solid lines: fitting curves).

The half-life crystallization time $t_{0.5}$, which is defined as the time at $X_t = 0.5$, is an important parameter for the discussion of crystallization kinetics. It can also be calculated using the equation:

$$t_{0.5} = (\frac{\ln 2}{k})^{1/n} \tag{7}$$

The half-life crystallization time $t_{0.5}$ can be either obtained directly from the curve of relative degree of crystallinity with time (Fig. 4) or calculated from isothermal parameter n and k by using Equation (7). These two sets of data are compared in Table 2. They are very close to each other for both neat PLLA and PLLA/CHAp within the range of crystallization temperatures. The value of $1/t_{0.5}$ can be used to describe the crystallization rate and is plotted in Fig. 5 as a function of isothermal crystallization temperature. As a typical semicrystalline polymer, the crystallization of PLLA is slow in temperature ranges close to the melting point and glass transition point. Di Lorenzo (2005) reported a discontinuity around 116-118 °C in a similar plot, which was ascribed to a sudden acceleration in spherulite growth. However, such discontinuity is not clear in Fig. 5. It can be seen that the crystallization rate of PLLA/CHAp was faster than neat PLLA. This implies that the nano-sized CHAp particles acted as an efficient nucleating agent. The highest overall isothermal crystallization rate was found between 100 to 110 °C. The increased crystallization rate due to the addition of CHAp into PLLA matrix was also confirmed by the higher values of isothermal crystallization parameter k listed in Table 2. Similar observations of inorganic particle reinforced PLLA composites exhibited increased bulk crystallization rates relative to neat polymer (Krikorian and Pochan 2004; Wu, Wu et al. 2007). This phenomenon is usually attributed to the higher heterogeneous nucleation rates, as demonstrated by increases in the isothermal crystallization parameter k. However, the effects of inorganic fillers on radial spherulite growth rates vary, depending on the properties and content of the fillers.

3.3 Crystal growth analysis by Lauritzen-Hoffman theory

The isothermal crystallization data obtained can be examined in terms of secondary nucleation or Lauritzen-Hoffman (LH) theory of polymer crystal growth (Hoffman, Davis et al. 1976). The growth face undergoes two different but related processes during polymer crystallization. One is the deposition of secondary nuclei on the growth face, and the other is the subsequent growth along the face at the sites where the secondary nuclei are formed. Therefore, there are two competing rates involved in the process that determine the regime in which the polymer crystallizes. On the basis of the secondary nuclei formation rate, *i*, and the lateral growth rate or the surface spreading rate, *g*, the crystallization regimes can be defined as follows:

$i << g$ Regime I

$i \sim g$ Regime II

$i >> g$ Regime III

Regime I, where *i* is much smaller than *g*, occurs at very low supercoolings (ΔT); Regime II, where *i* is in the order of *g*, occurs at moderate ΔT; and Regime III, where *i* is much greater than *g*, occurs at very high ΔT (Patki, Mezghani et al. 2007). Thus Regime I is characterized by mononucleation of the nucleus on a substrate, followed by lateral spreading or growth of a chain-folded crystal lamella. The linear growth rate is controlled by secondary nucleation in Regime I. In contrast, Regime II occurs by multiple nucleations at lower crystallization temperatures (Tjong and Bao 2005). As the temperature is further lowered, prolific and

multiple nucleation can occur in Regime III (Pethrick 2007). Most polymers exhibit different regime behavior, depending on the crystallization condition.

LH theory assumes that a free energy barrier associated with nucleation has an energetic origin and it provides the general expression for the growth rate (G) of a linear polymer crystal with folded chains:

$$G = G_0 \exp[\frac{-U^*}{R(T_c - T_\infty)}]\exp(\frac{-K_g}{T_c \Delta T f}) \tag{8}$$

where K_g is the nucleation constant (for details see Equation (11)); ΔT is the undercooling defined by $T_m^0 - T_c$; T_m^0 is the equilibrium melting point which is 479.2K for PLLA (Iannace and Nicolais 1997); f is a factor given as $2T_c / (T_m^0 + T_c)$; U^* is the activation energy for polymer diffusion which means the transportation of segments to the crystallization site, and the universal value of U^* = 1500 cal/mol (6276 J/mol) was used in order to compare the results from literature (Iannace and Nicolais 1997); R is the gas constant [8.314 J/(mol K)]; T_∞ is the hypothetical temperature where all motion associated with viscous flow ceases and normally chosen as T_g-30K; and G_0 is the front factor.

Using a theoretical approach, it can be shown that the linear growth rate G can be considered proportional to $1/t_{0.5}$. Based on the LH theory (Hoffman and Miller 1997), the temperature variation of $1/t_{0.5}$ can be written as:

$$(\frac{1}{t_{0.5}}) = (\frac{1}{t_{0.5}})_0 \exp[\frac{-U^*}{R(T_c - T_\infty)}]\exp(\frac{-K_g}{T_c \Delta T f}) \tag{9}$$

It should be pointed out that this is only an approximation. Ideally, the value of spherulite growth rate (G) should be measured directly by optical microscopy and equation (8) be applied. However, the spherulites of the PLLA/CHAp nanocomposite were too small and accurate measurements of their growth rate were not possible. Second, the G values measured by optical microscopy are obtained under a confined 2D environment, i.e. the spherulites will grow between two microscope cover slides. Also, there is doubt whether limited number of 2D measurements can really represent the true 3D spherulite growth in large number. On the other hand, DSC analysis allows 3D polymer spherulite growth and the data will give a more macro-scale representation of the real situation.

For practical convenient use, Equation (9) is usually rewritten as

$$\ln(\frac{1}{t_{0.5}}) + \frac{U^*}{R(T_c - T_\infty)} = \ln(\frac{1}{t_{0.5}})_0 - \frac{K_g}{T_c \Delta T f} \tag{10}$$

The plot of the left-hand side of Equation (10) vs. $1/T_c\Delta T_f$ gives the slope of $-K_g$ from which the nucleation constant K_g can be evaluated. In the current investigation, U^*= 6276 J/mol, as stated earlier, was used in the plot (Fig. 6). For both neat PLLA and PLLA/CHAp, there were two crystallization regimes, i.e. Regimes II and III, in the isothermal temperature range. From Fig. 6, the K_g (II) values for neat PLLA and PLLA/CHAp were estimated to be 5.74×10^5 and 4.76×10^5, respectively, within the T_c range of 120-140 °C (Table 3). The K_g (II) value for neat PLLA was higher than those reported in the literature, including 2.92×10^5

based on isothermal crystallization parameters (Iannace and Nicolais 1997) and 3.01×10^5 on spherulite growth rate *G* values (Tsuji, Takai et al. 2006). K_g (III) for neat PLLA obtained here was 9.02×10^5 which was similar to 8.91×10^5 as reported by Iannace and Nicolais (1997) and 9.00×10^5 by Tsuji et al. (2006). According to Iannace and Nicolais (1997), the theoretical value of the ratio K_g (III)/K_g (II) is 2. In the current investigation, the respective ratios for neat PLLA and PLLA/CHAp were 1.57 and 1.74. The lower values obtained here could be related to either the different sets of values utilized for U^* and T_∞ or the difference in molecular weight of polymers used.

The transition from Regime II to Regime III was observed at about 120 °C for both neat PLLA and PLLA/CHAp, which was in agreement with the results obtained using *G* values (Iannace and Nicolais 1997; Abe, Kikkawa et al. 2001; Tsuji, Miyase et al. 2005; Tsuji, Takai et al. 2006). This indicates that the LH theory is a valid method to predict nucleation constant if the Avrami fit is good. The current investigation shows that the addition of CHAp nanoparticles did not alter the transition temperature of PLLA crystallization from Regime II to Regime III but caused a reduction in the value of K_g. The lower K_g for PLLA/CHAp suggests that less energy was needed for the formation of critical size of PLLA nuclei in the nanocomposite than in the neat PLLA.

The nucleation constant K_g in Equation (8) is given by:

$$K_g = \frac{Zb_0\sigma\sigma_e T_m^0}{\Delta h_f k_B} \tag{11}$$

where σ is the lateral surface free energy, σ_e is the fold surface energy , b_0 is the layer thickness of the crystal, Δh_f is the volumetric heat of fusion and k_B is the Boltzmann constant. The value of Z is dependent on the crystallization regime and equal to 4 for Regimes I (high temperatures) and III (low temperatures) and values 2 for Regime II (intermediate temperatures) (Di Lorenzo 2005). In the current investigation, the K_g values were used to calculate the fold surface free energy according to Equation (11). The lateral surface energy was determined by the Thomas-Stavely empirical equation (Hoffman, Davis et al. 1976):

$$\sigma = \alpha_0 \Delta h_f \sqrt{a_0 b_0} \tag{12}$$

where α_0 is an empirical constant and usually assumed to be 0.25 which is appropriate to high melting polyesters (Qiu and Yang 2006); represents the cross-sectional area of PLLA chains, with =5.97×10^{-10} m and =5.17×10^{-10} m from the literature; and Δh_f=1.11×10^8 J/m^3 (Di Lorenzo 2001). The σ value was then calculated to be 15.4×10^{-3} J/m^2, and which was close to the reported data (Krikorian and Pochan 2004). The values of fold surface energy σ_e were obtained by solving Equation (11) and are listed in Table 3. For neat PLLA, the value of σ_e varies in the range of 91-117 erg/cm^2 (1 erg/cm^2= 1×10^{-3} J/m^2), which agrees well with the result (107 erg/cm^2) by Miyata and Masuko (1998) but higher than 40.5 erg/cm^2 by Di Lorenzo (2001) and 43.5 erg/cm2 by Wu et al. (2007). It has been shown that the value of σ_e is dependent on the molecular weight of PLLA (Miyata and Masuko 1998) and the cooling or heating rate to the isothermal crystallization temperature (Wu, Wu et al. 2007). Miyata and Masuko (1998) implied that the value of σ_e increases with increase in the loose-loop chains on the fold surface of high molecular weight PLLA. The decrease of σ_e with

increasing heating rate was considered by Wu et al. (2007) due to the change of nucleation mechanism from Regime III to Regime II by Lauritzen-Hoffman-Miller analysis. However, they did not show the transition temperature from Regime III to Regime II.

Samples	K_g (III) (K^2)	σ_e (III) (J/m^2)	q (III) (kJ/mol)	K_g (II) (K^2)	σ_e (II) (J/m^2)	q (II) (kJ/mol)
PLLA	9.02×10^5	91×10^{-3}	33.8	5.74×10^5	117×10^{-3}	43.5
PLLA/CHAp	8.36×10^5	84×10^{-3}	31.2	4.79×10^5	96×10^{-3}	35.7

Table 3. Lauritzen-Hoffman parameters for isothermal crystallization of neat PLLA and PLLA/CHAp nanocomposite.

It can be seen from Table 3 that addition of CHAp nanoparticles decreased the values of σ_e for PLLA by 18% in Regime II and 7.7% in Regime III. The lower values of the free energy of chain folding of the lamellar crystals in PLLA/CHAp suggest that the CHAp nanoparticles facilitated the crystallization of PLLA. According to Wittmann and Lotz (1990), the incorporation of nucleating agents into polymers changes the polymer crystallization behavior. Heterogeneous nucleating agents, such as filler particles and fibers, tend to promote the nucleation of spherulites on their surfaces, decrease the lamellar thickness and lead to epitaxial growth of crystallites. In this study, the nucleating ability of the CHAp has been clearly shown in Fig. 7 but the latter two mechanisms have not been examined.
Finally, the work for chain folding, q, which means by bending the polymer chain back upon itself in the appropriate configuration and is apparently correlated with molecular structure, can be expressed as follows (Patki, Mezghani et al. 2007):

$$q = 2a_0 b_0 \sigma_e \tag{13}$$

The values of q in Regime II and Regime III for neat PLLA and PLLA/CHAp nanocomposite were determined and are listed in Table 3. It was found that the values of q for neat PLLA were higher than those for PLLA/CHAp in both Regime II and Regime III. q is a measure of the inherent stiffness of polymer chain: more flexible chains have smaller values of q, and vice versa (Runt, Miley et al. 1992). The results show that the CHAp nanoparticles reduced the work needed for PLLA chains to fold into the crystal. Such phenomenon may arise due to a reduced size or a lower degree of perfection of the crystals formed.

3.4 Spherulite morphology

The spherulitic morphologies of neat PLLA and PLLA/CHAp nanocomposite were investigated using polarized optical microscopy at selected crystallization temperatures of 110, 120 and 130 °C and the results are shown in Fig. 7 (a-f). Since sufficient time was given for crystallization, according to the isothermal crystallization kinetics study, both neat PLLA and PLLA/CHAp were completely crystallized. It can be seen from Fig. 7 that the spherulites of neat PLLA were distinctive and of considerable size while those of PLLA/CHAp were much smaller and less distinctive. This clearly shows that the nano-sized CHAp acted as an effective nucleating agent to induce a great number of additional nuclei but, on the other hand, it also limited the growth space for each nucleus, leading to the

formation of smaller spherulites. In the theoretical approach for growth rate analysis, the Lauritzen-Hoffman equation can be applied using half-time of crystallization ($t_{0.5}$) under the assumption that the crystallization rates are inversely proportional to $t_{0.5}$. This theoretical approach has been widely used in crystallization study of both neat polymers and their composite systems (Iannace and Nicolais 1997; Tsuji, Takai et al. 2006; Chen, Yao et al. 2007; Liao, Yang et al. 2007; Wu, Wu et al. 2007). It is shown in Fig. 5 that the values of $1/t_{0.5}$ for the PLLA/CHAp nanocomposite were higher than those of the neat PLLA, which means the nanocomposite has a higher crystallization rate than the neat polymer.

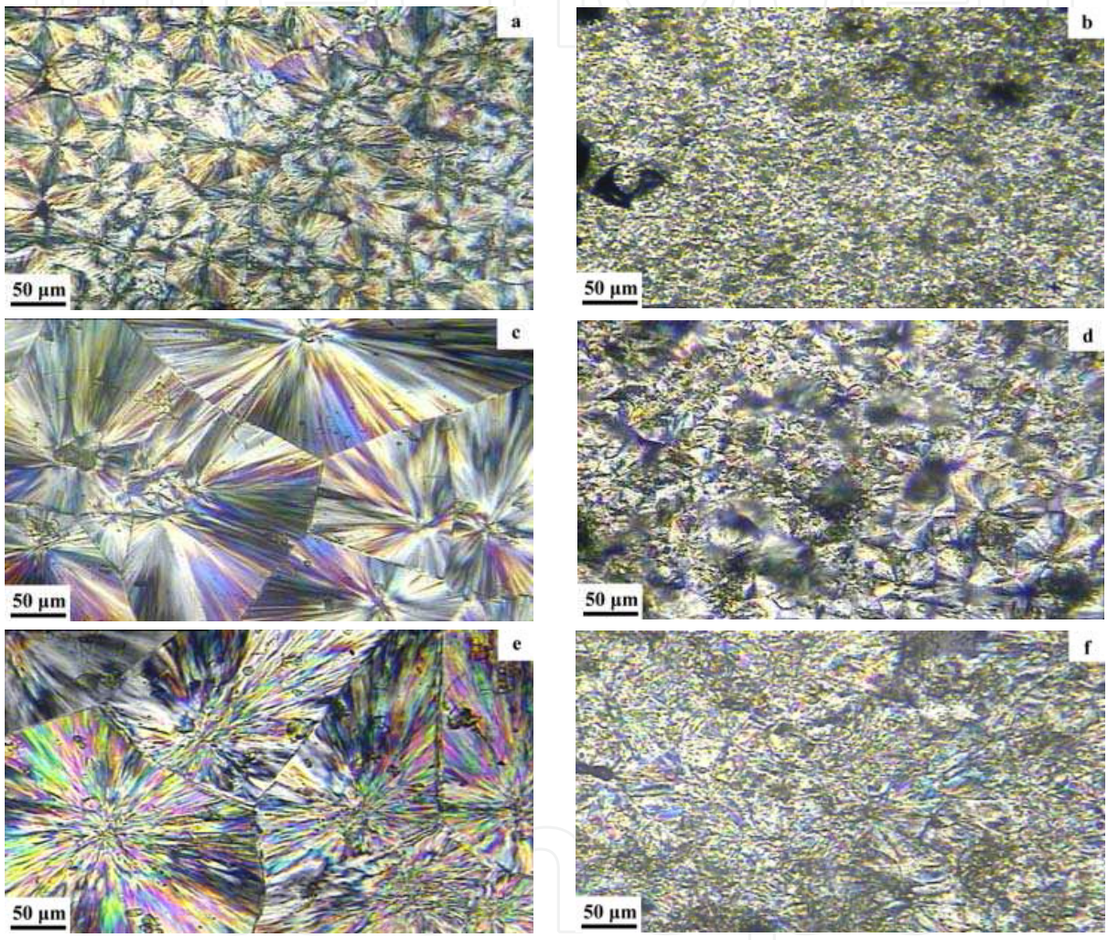

Fig. 7. Polarized optical micrographs showing the spherulitic morphologies of neat PLLA and PLLA/CHAp crystallized at various temperatures: (a) neat PLLA at 110 °C for 50 min, (b) PLLA/CHAp at 100 °C for 30 min, (c) neat PLLA at 120 °C for 90 min, (d) PLLA/CHAp at 120 °C for 40 min, (e) neat PLLA at 130 °C for 180 min, (f) PLLA/CHAp at 130 °C for 70 min. (* Fig c was selected in the book "Physical Metallurgy and Advanced Materials", eds by R.E. Smallman & A.H.W. Ngan, 7th edition, P557.)

3.5 Non-isothermal crystallization kinetics

The non-isothermal crystallization thermograms for neat PLLA and PLLA/CHAp nanocomposites obtained at six cooling rates are shown in Fig. 8. From these curves, useful

crystallization parameters such as the peak temperature (T_p), at which the sample has the fastest crystallization, can be determined and used for further calculations. It can be seen that the crystallization enthalpy first increased and then decreased with increasing cooling rates. This phenomenon was also reported by Chen et al. (Chen, Fei et al. 2002) in the non-isothermal crystallization study of maleated poly(3-hydroxybutyrate). The crystallization enthalpy reached a maximum at about 2.5 °C/min for neat PLLA and 5 °C/min for PLLA/CHAp is caused by crystallization in the α′ polymorph, that causes a drastic increase of crystallization rate below 120 °C.

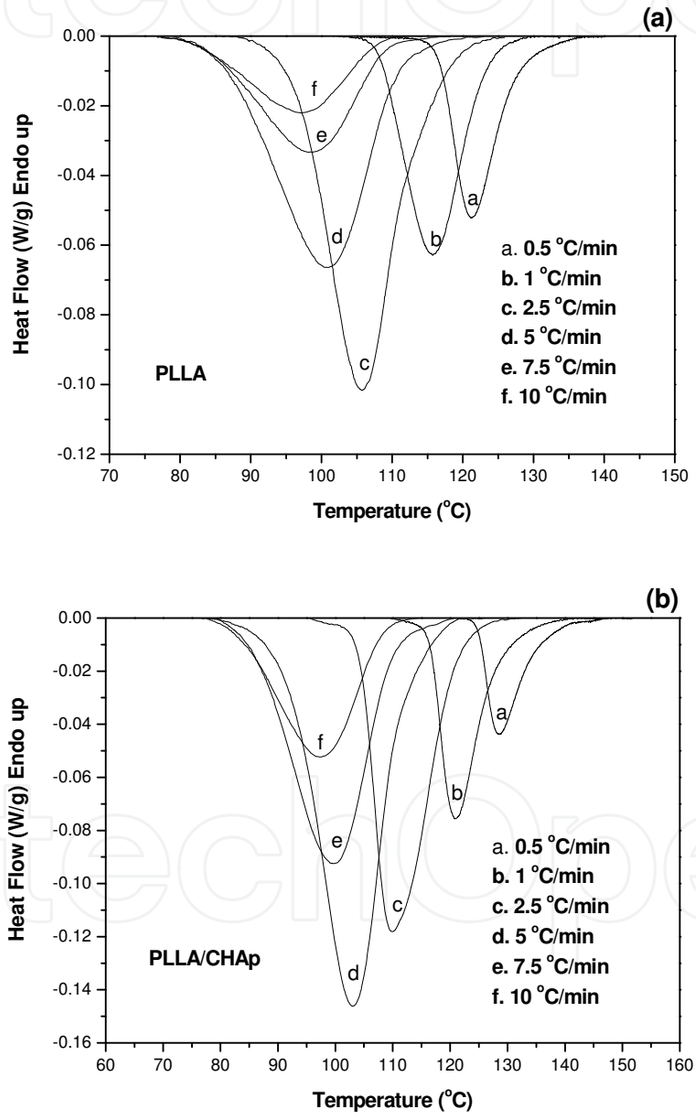

Fig. 8. DSC thermograms obtained from non-isothermal crystallization of (a) neat PLLA, and (b) PLLA/CHAp nanocomposites. (Cooling rates are indicated in the graphs.)

Ozawa (1971) extended the Avrami equation for the non-isothermal crystallization analysis. Assuming that the non-isothermal crystallization process is composed of infinitesimally

small isothermal crystallization steps, the relative volumetric crystallinity X_t at temperature T can be calculated as follows:

$$X_t = 1 - \exp[\frac{-K(T)}{\phi^m}] \tag{14}$$

or

$$\log[-\ln(1 - X_t)] = \log K(T) + m \log \phi^{-1} \tag{15}$$

where *m* is the Ozawa exponent, which depends on the dimensions of the crystal growth, and *K(T)* is a function of cooling rate ϕ and indicates how fast crystallization occurs. If the Ozawa method is valid, plots of $\log[-\ln(1-X_t)]$ versus $\log \phi^{-1}$ should be straight lines, and kinetic parameters *K(T)* and *m* should be obtainable from the intercept and slope of the lines, respectively. However, when the cooling rates vary in a large range, the poor linearity of the plots renders the results calculated from Equation (14) questionable. Moreover, the assumption of constant cooling rates may cause problems in modeling the change of crystallinity during polymer processing (Di Lorenzo and Silvestre 1999). The Ozawa theory neglects the slow secondary crystallization and the dependence of lamellar thickness on the temperature so that it cannot describe the full process of non-isothermal crystallization of polymers in general (Lee and Cakmak 1998; Di Lorenzo and Silvestre 1999; Kim, Ahn et al. 2003; Jain, Goossens et al. 2005; Wu, Wu et al. 2007).

Aiming to find a method to describe exactly the non-isothermal crystallization process, a combination of Avrami and Ozawa equations was proposed recently (Liu, Mo et al. 1997). During the non-isothermal crystallization process, the relationship between crystallization time t and temperature T is given by

$$t = \frac{T_0 - T}{|\phi|} \tag{16}$$

where T is the temperature at time t, T_0 is the initial temperature when crystallization begins (t = 0). The Avrami equation relates X_t with time t, and the Ozawa equation relates X_t with cooling rate ϕ, thus the relationship between ϕ and t can be established to connect these two equations as follows:

$$\log \phi = \log F(T) - \alpha \log t \tag{17}$$

where the rate parameter $F(T) = [\frac{K(T)}{k}]^{1/m}$ and the physical meaning is the necessary value of cooling rate to reach a defined degree of crystallinity at unit crystallization time; α is the ratio of the Avrami exponent n to the Ozawa exponent m, i.e., α = n/m. According to Equation (17), at a given degree of crystallinity, the plot of $\log \phi$ as a function of $\log t$ gives a straight line with $\log F(T)$ as the intercept and $-\alpha$ as the slope. The combined Ozawa-Avrami model actually is a modified model in which crystallization functions are related to certain X_t values. This method is more convenient in the analysis of non-isothermal crystallization

process, but it needs to be considered with care about its physical meaning (Buzarovska, Bogoeva-Gaceva et al. 2007).

Fig. 9 presents the relative degree of crystallinity as a function of time for neat PLLA and PLLA/CHAp crystallized at various cooling rates. The higher the cooling rate, the shorter time range within which crystallization occurs. The retardation effect of cooling rate on the crystallization is observed only at low cooling rates (<5 °C/min), below which the X_t–t curve shows an obvious S shape. At higher cooling rates, melted PLLA evolves into the glassy state quickly and hence the X_t–t curve tends to straight.

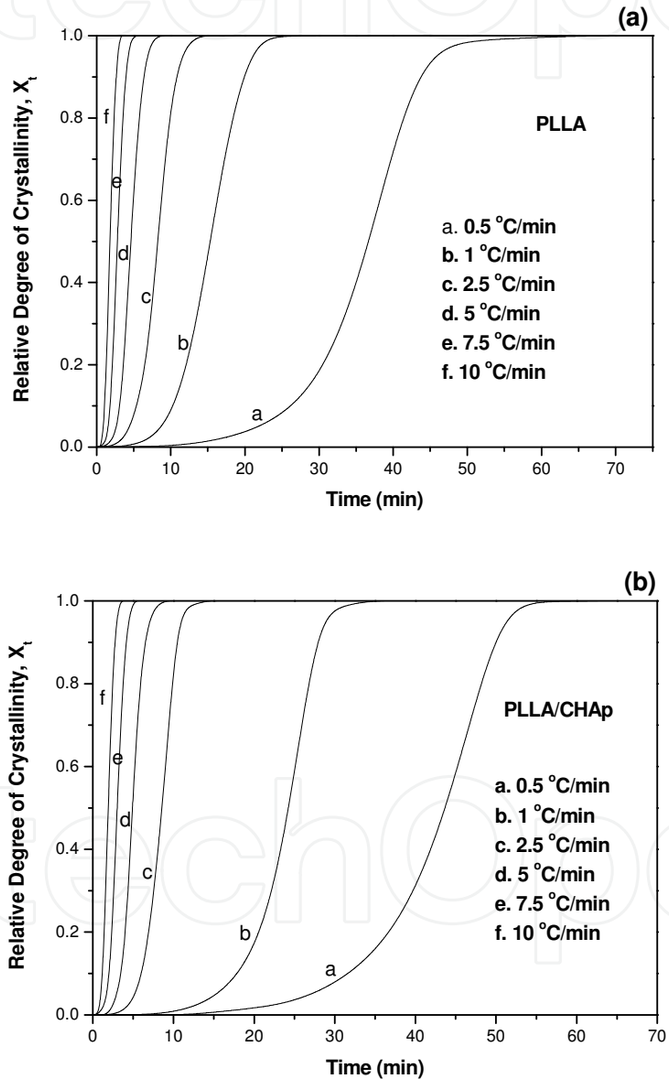

Fig. 9. Plots of relative degree of crystallinity as a function of time for (a) neat PLLA, and (b) PLLA/CHAp nanocomposite.

Fig. 10 presents the plots of log ϕ as a function of log t for neat PLLA and PLLA/CHAp. The good linearity of the plots demonstrates the good applicability of the combined Avrami-Ozawa method in the current investigation. Values of *F(T)* and α are listed in Table 4, from

which it can be seen that the values of *F(T)* increase systematically with an increase in the relative degree of crystallinity. Thus, at a unit crystallization time, a higher cooling rate is needed to achieve a higher degree of crystallinity. *F(T)* is considered as a parameter that indicates the polymer crystallization rate. A lower *F(T)* value means a higher crystallization rate under non-isothermal crystallization condition (Huang, Gu et al. 2006). The PLLA/CHAp nanocomposite had a larger *F(T)* value than neat PLLA in the low X_t range (<0.40), while the trend was opposite in the high X_t range (≥0.40). This indicates that the addition of CHAp only accelerated the PLLA crystallization rate in the initial crystallization stage. The values of parameter α are nearly constant and close to 1 which means that the Avrami exponent and Ozawa exponent are more or less the same for both neat PLLA and PLLA/CHAp.

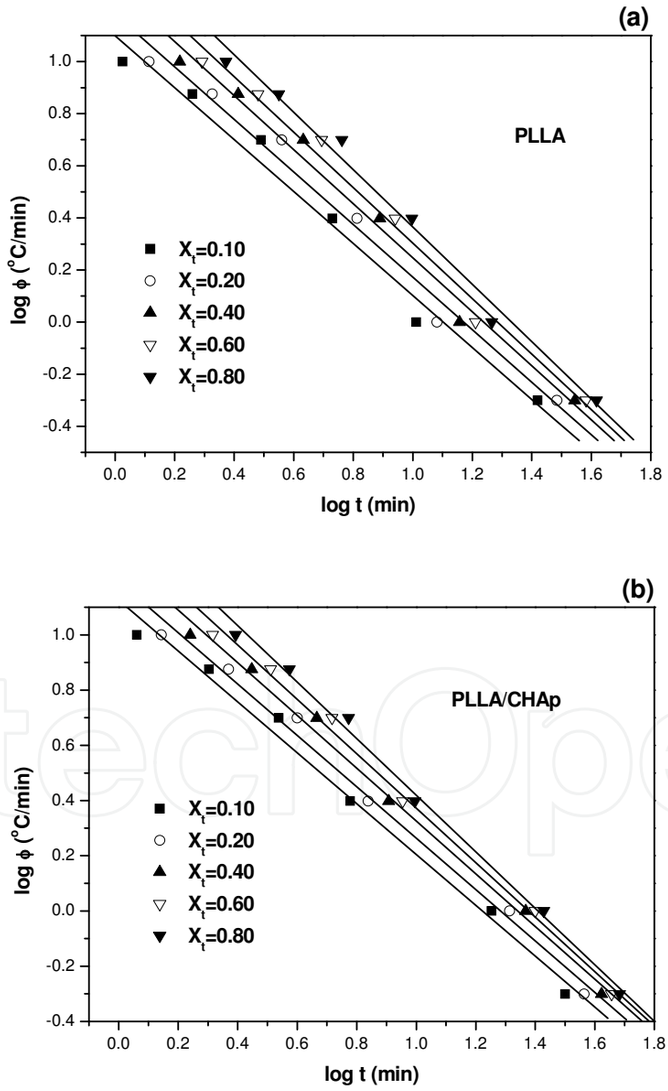

Fig. 10. Plots of log ϕ as a function of log t for (a) neat PLLA and (b) PLLA/CHAp nanocomposite based on combined Ozawa-Avrami equation.

Fig. 11 shows the relation between cooling rate (ϕ) and peak crystallization temperature (T_p) for neat PLLA and PLLA/CHAp. The T_p values for both neat PLLA and PLLA/CHAp shift to a lower temperature as the cooling rate increases. T_p value of PLLA/CHAp is higher than that of neat PLLA at the same cooling rate, indicating that the addition of CHAp accelerates the PLLA crystallization.

X_t	PLLA			PLLA/CHAp		
	α	F(T)	r^2	α	F(T)	r^2
0.10	1.00	12.59	0.9820	0.92	13.49	0.9898
0.20	1.01	15.14	0.9837	0.93	15.49	0.9917
0.40	1.04	19.50	0.9867	0.96	19.06	0.9940
0.60	1.06	23.44	0.9880	0.99	22.91	0.9951
0.80	1.10	29.51	0.9887	1.02	27.54	0.9956

r^2 denotes the coefficient of determination of Fig. 10.

Table 4. Values of *F(T)* and α obtained from the combined Avrami-Ozawa equation for neat PLLA and PLLA/CHAp nanocomposite.

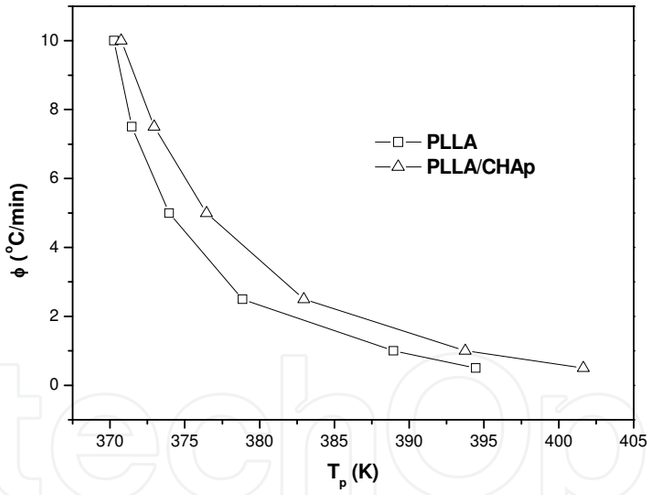

Fig. 11. Plots of cooling rate ϕ as a function of peak crystallization temperature T_p for PLLA and PLLA/CHAp nanocomposites.

3.6 Effective activation energy of non-isothermal crystallization

The crystallization activation energy during non-isothermal processes for neat PLLA and PLLA/CHAp can be evaluated using the Kissinger equation (Kissinger 1956):

$$\frac{d[\ln(\varphi / T_p^{\,2})]}{d(1/T_p)} = -\frac{\Delta E_C}{R} \tag{18}$$

where ΔE_C is the crystallization activation energy and *R* is the gas constant. The activation energy ΔE_C can be obtained from the slope of the plot of $\ln(\phi/T_p^2)$ versus $1/T_p$ which is presented in Fig. 12 for neat PLLA and PLLA/CHAp, respectively. The calculated ΔE_C for neat PLLA and PLLA/CHAp are -149.67 and -124.91 kJ/mol, respectively. ΔE_C values are negative, indicating that the rate of crystallization increased with decreasing temperature and the crystallization process of polymer is a barrierless and spontaneous process (the lower value of ΔE_C, the faster of crystallization rate) (Ma, Hu et al. 2007). The obtained crystallization activation energy of neat PLLA fits well with the reported value of -146.86 kJ/mol (Hao, Li et al. 2005).

There are other methods for obtaining the activation energy from non-isothermal crystallization, such as the Augis-Bennett method (Augis and Bennett 1978) and the Takhor method (Takhor 1971). But the Kissinger method appears to be the most popular method for evaluating ΔE_C. However, all these three methods involve the cooling rate ϕ but its negative sign has been omitted in the logarithm formulation. Recently, Vyazovkin (2002) demonstrated that dropping the negative sign for ϕ is a mathematically invalid procedure that generally makes the Kissinger type equation inapplicable to melt crystallization.

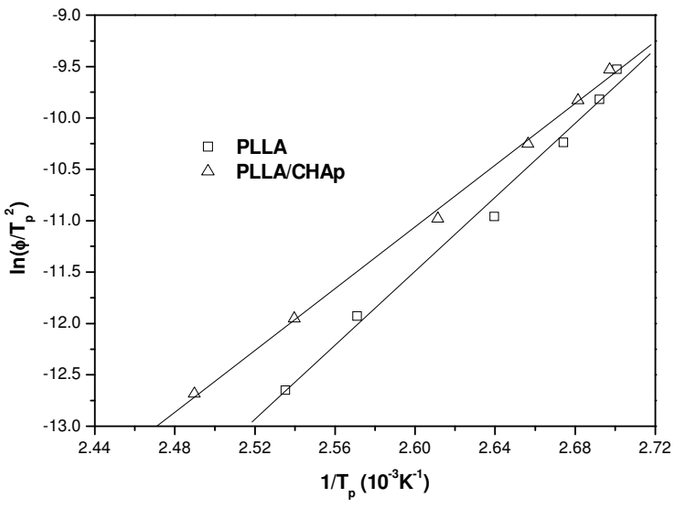

Fig. 12. Plots of $\ln(\phi/T_p^2)$ as a function of $1/T_p$ for neat PLLA and PLLA/CHAp nanocomposite.

Another disadvantage is that only a single value of activation energy is used for multiple non-isothermal crystallization processes by Kissinger-type methods. However, the crystallization rate is determined by the rates of nucleation and growth, whose activation energies are likely to be different. Sánchez-Jiménez et al. (2008) demonstrated that the Kissinger method only valid when the reaction obeys a first order kinetic law. In order to overcome the disadvantages of Kissinger-type methods, an isoconversion method can be applied to non-isothermal crystallization for evaluating the dependence of the activation energy on crystallinity and temperature. The representative methods include the differential isoconversion method (Friedman 1964) and the advanced integral isoconversion method (Vyazovkin and Sbirrazzuoli 2006). In the current investigation, the numerical differential method by Friedman (1964) was used. According to Friedman, different effective activation energies are calculated for every degree of crystallinity using the following equation:

$$\ln\left(\frac{dX}{dt}\right)_{X,i} = Const - \frac{\Delta E_X}{RT_{X,i}} \tag{19}$$

where dX/dt is the instantaneous crystallization rate as a function of time at a given crystallinity X, ΔE_X is the effective activation energy at given crystallinity X, $T_{X,i}$ is the set of temperatures related to a given crystallinity X at different cooling rates and the subscript i refers to every individual cooling rate used. The instantaneous crystallization rate, dX/dt, can be obtained from Fig. 9 by differentiation. Furthermore, by selecting appropriate degrees of crystallinity (i.e., from 10 to 90%) the values of dX/dt at a specific X are correlated to the corresponding crystallization temperature, T_X. Then by plotting dX/dt with respect to $1/T_X$, a straight line should be obtained with a slope equal to $\Delta E_X/R$.

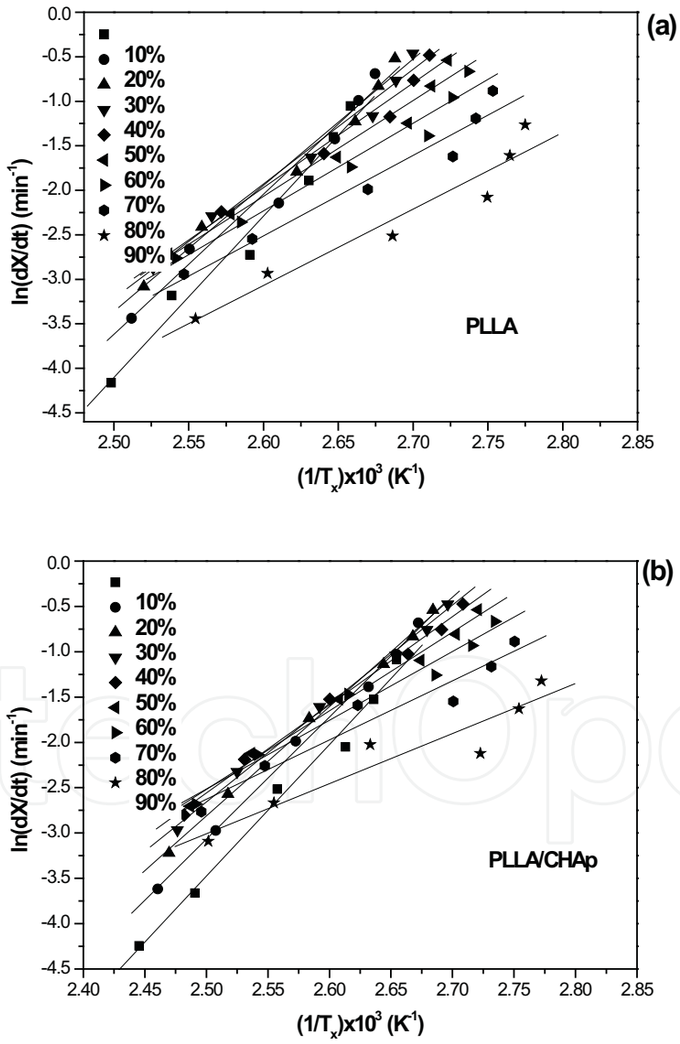

Fig. 13. Friedman plots of ln(dX/dt) vs. $1/T_x$ for (a) neat PLLA and (b) PLLA/CHAp nanocomposite at different relative degrees of crystallinity. The solid lines represent the linear fits.

Fig. 13 shows Friedman plots for neat PLLA and PLLA/CHAp nanocomposites at different relative degrees of crystallinity. The straight lines obtained were used to calculate the effective activation energies of neat PLLA and PLLA/CHAp which are shown in Fig. 13. As can be seen, the effective activation energy increased with the increase in the relative degree of crystallinity for all neat PLLA and PLLA/CHAp. In all cases, the absolute values of ΔE_X for PLLA was higher than that for PLLA/CHAp, indicating that the CHAp nanoparticles (10 wt%) lower the non-isothermal crystallization rate of PLLA. Interestingly, the values of activation energy obtained by the Kissinger method for both PLLA and PLLA/CHAp also fall on the curves in Fig. 14 at the relative degree of crystallinity near 10%. This indicates that the Kissinger method may represent one case in the ΔE_X dependence of crystallinity by the Friedman method.

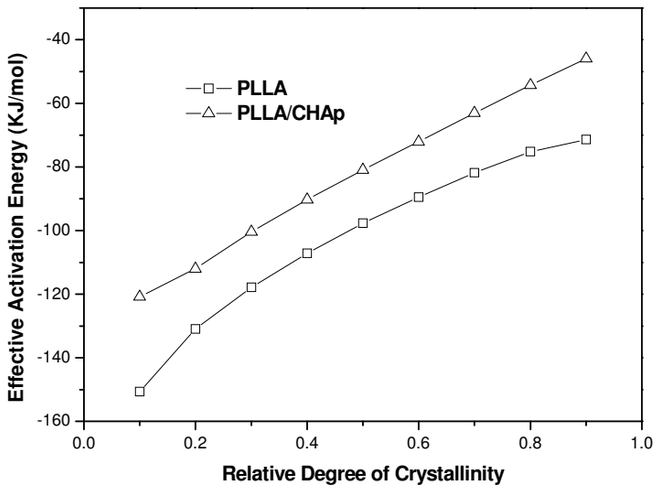

Fig. 14. Dependence of effective activation energy on relative degree of crystallinity in non-isothermal crystallization of PLLA and PLLA/CHAp nanocomposite.

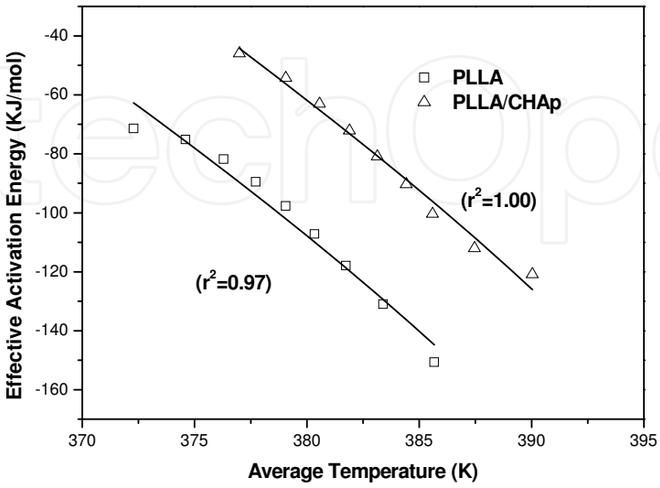

Fig. 15. Dependence of effective activation energy on average temperature for PLLA and PLLA/CHAp nanocomposite. The solid lines represent the nonlinear fits.

Furthermore, the relative degree of crystallinity is dependent on the non-isothermal crystallization temperature. Thus the effective activation energy can be plotted as a function of temperature by taking an average crystallization temperature associated with a certain relative degree of crystallinity (Papageorgiou, Achilias et al. 2007). The symbols in Fig. 15 display the ΔE_X –T relationship for neat PLLA and PLLA/CHAp, respectively. Vyazovkin and Sbirrazzuoli (2004) recently derived an equation to correlate the dependence of effective activation energy on temperature in terms of the Lauritzen-Hoffman parameters (U* and K_g):

$$E_X(T) = U^* \frac{T^2}{(T - T_\infty)^2} + K_g R \frac{T_m^{0\,2} - T^2 - T_m^0 T}{(T_m^0 - T)^2 T} \tag{20}$$

In the current investigation, the graphics software Origin® (Microcal Software, Inc) was employed to perform the nonlinear fits of Equation (20) and the results are shown as the solid lines in Fig. 15. The values of T_∞ and T_m^0 used were the same as those in Section 3.3. The values of U* and K_g yielded by the fits are shown in Table 5. The coefficients of determination (r^2) were found to be 0.97 and 1.00 for neat PLLA and PLLA/CHAp, respectively. The K_g values were similar to the values obtained from the isothermal crystallization analysis for Regime III, i.e. for crystallization temperatures below 120 °C (refer to Section 3.3). However, the regime transition was not observed due to the limited temperature intervals in the non-isothermal crystallization experiment. The obtained values of U* were much lower than the commonly used value of 6276 kJ/mol. This indicates that the commonly used value of U* may not be applicable to all polymers. The current analysis has demonstrated that the parameters of the Lauritzen-Hoffman equation can be obtained from DSC data on the overall rates of non-isothermal crystallization. In fact, this method have been successfully applied to the non-isothermal crystallization of a poly(ethylene terephthalate) (PET) with medium to slow crystallization rates by Vyazovkin and Sbirrazzuoli (2004), poly(propylene terephthalate) (PPT) and poly(butylene 2,6-naphthalate) (PBN) with fast crystallization rates by Achilias et al (2005) and nanocomposites of polyamide 6/halloysite nanotube recently by Guo et al (2009). In the current investigation, the validity of using the Vyazovkin-Sbirrazzuoli method for PLLA and PLLA/CHAp nanocomposite has been demonstrated.

Samples	U^* (J/mol)	K_g (III) (K^2)	Coefficient of Determination, r^2
PLLA	1846	7.52×10^5	0.97
PLLA/CHAp	2565	6.37×10^5	1.00

Table 5. Lauritzen-Hoffman parameters for neat PLLA and PLLA/CHAp nanocomposite obtained through isoconversion analysis of their non-isothermal crystallization.

4. Conclusions

The following conclusions can be drawn from the investigation into the effects of inclusion of CHAp nanoparticles on thermal properties, isothermal and non-isothermal melt crystallization kinetics of PLLA (Zhou, Duan et al. 2009):

1. The addition of 10 wt% of CHAp decreased the glass transition temperature and cold crystallization temperature of PLLA and slightly increased the melting temperature of PLLA. When cooled rapidly (50 °C/min) from the melt, the neat PLLA remained amorphous while PLLA/CHAp exhibited a crystallinity of 4%, which was probably caused by induced heterogeneous nucleation due to the presence of CHAp nanoparticles.
2. At high isothermal crystallization temperatures, the addition of CHAp decreased the crystallization enthalpy significantly compared with that of neat PLLA. Such changes imply a drop in the amount of crystals formed or a lower degree of perfection of the crystals. The Avrami equation described the isothermal crystallization kinetics well for both neat PLLA and PLLA/CHAp. The Avrami exponent n for neat PLLA and PLLA/CHAp approached 3 when increasing the isothermal crystallization temperature to 140°C, which indicates a three-dimensional crystal growth. The maximum isothermal crystallization rate was found to be between 100 to 110 °C.
3. By using Lauritzen-Hoffman theory, the nucleation constant (K_g), the fold surface energy (σ_e) and the work of chain folding (q) for neat PLLA and PLLA/CHAp could be obtained. The transition temperature from Regime II to Regime III was found to be about 120 °C for both neat PLLA and PLLA/CHAp. The CHAp nanoparticles acted as an efficient nucleating agent, thus increasing the nucleation rate and decreasing the fold surface energy of PLLA. The nucleating agent effect of CHAp was also confirmed by the observations of smaller spherulites in PLLA using polarized optical microscopy.
4. The non-isothermal crystallization kinetics of neat PLLA and PLLA/CHAp nanocomposite were investigated with DSC at cooling rates range from 0.5 to 10 °C/min. The combined Avrami-Ozawa equation was applied to analyze the non-isothermal crystallization process and the Ozawa exponent for neat PLLA and PLLA/CHAp were found to be very close to their Avrami exponent. According to the data obtained, the addition of CHAp only promoted the PLLA crystallization rate in the initial crystallization stage due to crystal germination under the non-isothermal condition. While in the isothermal condition, the addition of CHAp nanoparticles had influences on both crystal germination and growth mainly in Regime II.
5. Using the Kissinger equation, the non-isothermal crystallization activation energies of neat PLLA and PLLA/CHAp were found to be -149.67 and -124.91 kJ/mol, respectively. The differential isoconversional method by Friedman was applied to further estimate the dependence of the effective activation energy on the relative crystallinity and temperature for PLLA and PLLA/CHAp under non-isothermal crystallization. The Lauritzen-Hoffman parameters were obtained from the non-isothermal crystallization data as well by using the Vyazovkin-Sbirrazzuoli equation, and the values of U^* and K_g for neat PLLA and PLLA/CHAp were found to be 1846 J/mol and 7.52×10^5 K², 2565 J/mol and 6.37×10^5 K², respectively.

5. Acknowledgements

This work was supported by a GRF research grant (HKU 7118/05E) from the Hong Kong Research Grants Council. Support by Prof. Bakr Rabie in the Faculty of Dentistry, HKU, is acknowledged.

6. References

Abe, H., Y. Kikkawa, et al. (2001). Morphological and kinetic analyses of regime transition for poly[(S)-lactide] crystal growth. *Biomacromolecules* 2(3): 1007-1014.

Achilias, D. S., G. Z. Papageorgiou, et al. (2005). Evaluation of the Isoconversional Approach to Estimating the Hoffman-Lauritzen Parameters from the Overall Rates of Non-Isothermal Crystallization of Polymers. *Macromolecular Chemistry and Physics* 206(15): 1511-1519.

Arnoult, M., E. Dargent, et al. (2007). Mobile amorphous phase fragility in semi-crystalline polymers: Comparison of PET and PLLA. *Polymer* 48(4): 1012-1019.

Augis, J. A. and J. E. Bennett (1978). Calculation of the Avrami parameters for heterogeneous solid state reactions using a modification of the Kissinger method. *Journal of Thermal Analysis and Calorimetry* 13(2): 283-292.

Buzarovska, A., G. Bogoeva-Gaceva, et al. (2007). Crystallization behavior of poly(hydroxybytyrate- co -valerate) in model and bulk PHBV/kenaf fiber composites. *Journal of Materials Science* 42(16): 6501-6509.

Chen, C., B. Fei, et al. (2002). Nonisothermal crystallization and melting behavior of poly(3-hydroxybutyrate) and maleated poly(3-hydroxybutyrate). *European Polymer Journal* 38(8): 1663-1670.

Chen, J. H., B. X. Yao, et al. (2007). Isothermal crystallization behavior of isotactic polypropylene blended with small loading of polyhedral oligomeric silsesquioxane. *Polymer* 48(6): 1756-1769.

Chen, Y., A. F. T. Mak, et al. (2006). PLLA scaffolds with biomimetic apatite coating and biomimetic apatite/collagen composite coating to enhance osteoblast-like cells attachment and activity. *Surface and Coatings Technology* 201(3-4): 575-580.

Di Lorenzo, M. L. (2001). Determination of spherulite growth rates of poly (l-lactic acid) using combined isothermal and non-isothermal procedures. *Polymer* 42(23): 9441-9446.

Di Lorenzo, M. L. (2005). Crystallization behavior of poly (l-lactic acid). *European Polymer Journal* 41(3): 569-575.

Di Lorenzo, M. L. and C. Silvestre (1999). Non-isothermal crystallization of polymers. *Progress in Polymer Science* 24(6): 917-950.

Friedman, H. L. (1964). Kinetics of thermal degradation of char-forming plastics from thermogravimetry. *J. Polym. Sci. Part C* 6: 183.

German, R. M. (1996). Introduction to Sintering. *Sintering Theory and Practice*. R. M. German. New York, Wiley: 8.

Guo, B., Q. Zou, et al. (2009). Crystallization behavior of polyamide 6/halloysite nanotubes nanocomposites. *Thermochimica Acta* 484(1-2): 48-56.

Hao, Q., F. Li, et al. (2005). Preparation and Crystallization Kinetics of New Structurally Well-Defined Star-Shaped Biodegradable Poly(L-lactide)s Initiated with Diverse Natural Sugar Alcohols. *Biomacromolecules* 6(4): 2236-2247.

Hoffman, J. D., G. T. Davis, et al. (1976). The rate of crystallization of linear polymers with chain folding. *Treatise on Solid State Chemistry*. N. B. Hannay. 3: 497.

Hoffman, J. D. and R. L. Miller (1997). Kinetics of crystallization from the melt and chain folding in polyethylene fractions revisited: theory and experiment. *Polymer* 38(13): 3151-3212.

Huang, H., L. Gu, et al. (2006). Non-isothermal crystallization and thermal transitions of a biodegradable, partially hydrolyzed poly (vinyl alcohol). *Polymer* 47(11): 3935-3945.

Iannace, S. and L. Nicolais (1997). Isothermal crystallization and chain mobility of poly(L-lactide). *Journal of Applied Polymer Science* 64(5): 911-919.

Ignjatovic, N., E. Suljovrujic, et al. (2004). Evaluation of Hot-Pressed Hydroxyapatite/Poly-L-lactide Composite Biomaterial Characteristics. *Journal of Biomedical Materials Research* 71(2): 284-294.

Jain, S., H. Goossens, et al. (2005). Effect of in situ prepared silica nano-particles on non-isothermal crystallization of polypropylene. *Polymer* 46(20): 8805-8818.

Kim, S. H., S. H. Ahn, et al. (2003). Crystallization kinetics and nucleation activity of silica nanoparticle-filled poly (ethylene 2, 6-naphthalate). *Polymer* 44(19): 5625-5634.

Kissinger, H. E. (1956). Variation of peak temperature with heating rate in differential thermal analysis. *Journal of Research of the National Institute of Standards and Technology* 57(4): 217-221.

Kolstad, J. J. (1996). Crystallization kinetics of poly(L-lactide-co-meso-lactide). *Journal of Applied Polymer Science* 62(7): 1079-1091.

Krikorian, V. and D. J. Pochan (2004). Unusual crystallization behavior of organoclay reinforced poly (L-lactic acid) nanocomposites. *Macromolecules* 37(17): 6480-6491.

Lee, S. W. and M. Cakmak (1998). Growth habits and kinetics of crystallization of poly (ethylene 2, 6-naphthalate) under isothermal and nonisothermal conditions. *Journal of Macromolecular Science, Part B* 37(4): 501-526.

Lever, T. (2007). Optimizing DSC experiments. *Thermal Analysis of Pharmaceuticcals*. D. Q. M. Craig and M. Reading. Boca Raton, CRC Press/Taylor & Francis: 30.

Liao, R. G., B. Yang, et al. (2007). Isothermal cold crystallization kinetics of polylactide/nucleating agents. *Journal of Applied Polymer Science* 104(1): 310-317.

Liu, T., Z. Mo, et al. (1997). Nonisothermal melt and cold crystallization kinetics of poly (aryl ether ether ketone ketone). *Polymer Engineering & Science* 37(3): 568-575.

Lorenzo, A. T., M. L. Arnal, et al. (2007). DSC isothermal polymer crystallization kinetics measurements and the use of the Avrami equation to fit the data: Guidelines to avoid common problems. *Polymer Testing* 26(2): 222-231.

Ma, Y., G. Hu, et al. (2007). Non-isothermal crystallization kinetics and melting behaviors of nylon 11/tetrapod-shaped ZnO whisker (T-ZnOw) composites. *Materials Science and Engineering: A* 460: 611-618.

Marega, C., A. Marigo, et al. (1992). Structure and Crystallization Kinetics of Poly(L-Lactic Acid). *Makromolekulare Chemie-Macromolecular Chemistry and Physics* 193(7): 1599-1606.

Miyata, T. and T. Masuko (1998). Crystallization behaviour of poly(L-lactide). *Polymer* 39(22): 5515-5521.

Murariu, M., A. Da Silva Ferreira, et al. (2007). Polylactide compositions. Part 1: Effect of filler content and size on mechanical properties of PLA/calcium sulfate composites. *Polymer* 48(9): 2613-2618.

Oca, H. M. d. and I. M. Ward (2007). Structure and mechanical properties of poly(L-lactic acid) crystals and fibers. *Journal of Polymer Science Part B: Polymer Physics* 45(8): 892-902.

Ozawa, T. (1971). Kinetics of non-isothermal crystallization. *Polymer* 12(3): 150-156.

Papageorgiou, G. Z., D. S. Achilias, et al. (2007). Crystallization Kinetics of Biodegradable Poly(butylene succinate) under Isothermal and Non-Isothermal Conditions. *Macromolecular Chemistry and Physics* 208(12): 1250-1264.

Patki, R., K. Mezghani, et al. (2007). Crystallization kinetics of polymers. *Physical Properties of Polymers Handbook*. J. E. Mark. New York, Springer: 626.

Pethrick, R. A. (2007). Polymer crystal growth. *Polymer structure characterization: from nano to macro organization*. Cambridge, UK, RSC Publishing: 158.

Piorkowska, E., A. Galeski, et al. (2006). Critical assessment of overall crystallization kinetics theories and predictions. *Progress in Polymer Science* 31(6): 549-575.

Qiu, Z. B. and W. T. Yang (2006). Crystallization kinetics and morphology of poly (butylene succinate)/poly (vinyl phenol) blend. *Polymer* 47(18): 6429-6437.

Runt, J., D. M. Miley, et al. (1992). Crystallization of poly (butylene terephthalate) and its blends with polyarylate. *Macromolecules* 25(7): 1929-1934.

Sánchez-Jiménez, P., J. Criado, et al. (2008). Kissinger kinetic analysis of data obtained under different heating schedules. *Journal of Thermal Analysis and Calorimetry* 94(2): 427-432.

Sosnowski, S. (2001). Poly (l-lactide) microspheres with controlled crystallinity. *Polymer* 42(2): 637-643.

Takhor, R. L. (1971). Advances in Nucleation and Crystallization of Glasses. *American Ceramics Society, Columbus*: 166-172.

Tjong, S. C. and S. P. Bao (2005). Crystallization regime characteristics of exfoliated polyethylene/vermiculite nanocomposites. *Journal of Polymer Science Part B: Polymer Physics* 43(3): 253-263.

Tsuji, H., T. Miyase, et al. (2005). Physical properties, crystallization, and spherulite growth of linear and 3-arm poly(L-lactide)s. *Biomacromolecules* 6(1): 244-254.

Tsuji, H., H. Takai, et al. (2006). Isothermal and non-isothermal crystallization behavior of poly(L-lactic acid): Effects of stereocomplex as nucleating agent. *Polymer* 47(15): 5430-5430.

Vyazovkin, S. (2002). Is the Kissinger Equation Applicable to the Processes that Occur on Cooling? *Macromolecular Rapid Communications* 23(13): 771-775.

Vyazovkin, S. and N. Sbirrazzuoli (2004). Isoconversional approach to evaluating the Hoffman-Lauritzen parameters(U* and Kg) from the overall rates of nonisothermal crystallization. *Macromolecular Rapid Communications* 25(6): 733-738.

Vyazovkin, S. and N. Sbirrazzuoli (2006). Isoconversional kinetic analysis of thermally stimulated processes in polymers. *Macromolecular Rapid Communications* 27(18): 1515-1532.

Wang, M. (2006). Composite Scaffolds for Bone Tissue Engineering. *American Journal of Biochemistry and Biotechnology* 2(2): 80-84.

Wei, G. and P. X. Ma (2004). Structure and properties of nano-hydroxyapatite/polymer composite scaffolds for bone tissue engineering. *Biomaterials* 25(19): 4749-4757.

Wittmann, J. C. and B. Lotz (1990). Epitaxial crystallization of polymers on organic and polymeric substrates. *Progress in Polymer Science* 15(6): 909-948.

Wu, D., L. Wu, et al. (2007). Nonisothermal Cold Crystallization Behavior and Kinetics of Polylactide/Clay Nanocomposites. *Journal of Polymer Science: Part B: Polymer Physics* 45: 1100-1113.

Zhou, W. Y., B. Duan, et al. (2009). Crystallization kinetics of poly(l-lactide)/carbonated hydroxyapatite nanocomposite microspheres. *Journal of Applied Polymer Science* 113(6): 4100-4115.

Zhou, W. Y., S. H. Lee, et al. (2007). Selective Laser Sintering of Tissue Engineering Scaffolds Using Poly(L-Lactide) Microspheres. *Key Engineering Materials* 334-335: 1225-1228.

Zhou, W. Y., S. H. Lee, et al. (2008). Selective laser sintering of porous tissue engineering scaffolds from poly(L-lactide)/carbonated hydroxyapatite nanocomposite microspheres. *Journal of Materials Science: Materials in Medicine* 19(7): 2535-2540.

Zhou, W. Y., M. Wang, et al. (2007). Fabrication and characterization of composite microspheres containing carbonated hydroxyapatite nanoparticles. *Key Engineering Materials* 334-335: 1221-1224.

Zhou, W. Y., M. Wang, et al. (2008). Synthesis of carbonted hydroxyapatite nanospheres through nanoemulsion. *Journal of Materials Science: Materials in Medicine* 19(1): 103-110.

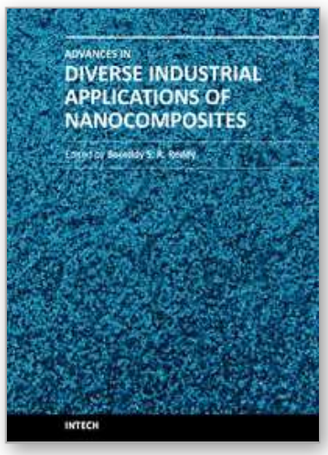

Advances in Diverse Industrial Applications of Nanocomposites
Edited by Dr. Boreddy Reddy

ISBN 978-953-307-202-9
Hard cover, 550 pages
Publisher InTech
Published online 22, March, 2011
Published in print edition March, 2011

Nanocomposites are attractive to researchers both from practical and theoretical point of view because of combination of special properties. Many efforts have been made in the last two decades using novel nanotechnology and nanoscience knowledge in order to get nanomaterials with determined functionality. This book focuses on polymer nanocomposites and their possible divergent applications. There has been enormous interest in the commercialization of nanocomposites for a variety of applications, and a number of these applications can already be found in industry. This book comprehensively deals with the divergent applications of nanocomposites comprising of 22 chapters.

How to reference
In order to correctly reference this scholarly work, feel free to copy and paste the following:

Wen You Zhou, Bin Duan, Min Wang and Wai Lam Cheung (2011). Isothermal and Non-isothermal Crystallization Kinetics of Poly(L-Lactide)/Carbonated Hydroxyapatite Nanocomposite Microspheres, Advances in Diverse Industrial Applications of Nanocomposites, Dr. Boreddy Reddy (Ed.), ISBN: 978-953-307-202-9, InTech, Available from: http://www.intechopen.com/books/advances-in-diverse-industrial-applications-of-nanocomposites/isothermal-and-non-isothermal-crystallization-kinetics-of-poly-l-lactide-carbonated-hydroxyapatite-n

INTECH
open science | open minds

InTech Europe
University Campus STeP Ri
Slavka Krautzeka 83/A
51000 Rijeka, Croatia
Phone: +385 (51) 770 447
Fax: +385 (51) 686 166
www.intechopen.com

InTech China
Unit 405, Office Block, Hotel Equatorial Shanghai
No.65, Yan An Road (West), Shanghai, 200040, China
中国上海市延安西路65号上海国际贵都大饭店办公楼405单元
Phone: +86-21-62489820
Fax: +86-21-62489821

IntechOpen